Solution Structure of *Ace*-AMP1, a Potent Antimicrobial Protein Extracted from Onion Seeds. Structural Analogies with Plant Nonspecific Lipid Transfer Proteins†

Séverine Tassin,*,‡ Willem F. Broekaert,§ Didier Marion,|| David P. Acland,⊥ Marius Ptak,‡,# Françoise Vovelle,‡,# and Patrick Sodano‡

Centre de Biophysique Moléculaire (CNRS) et Université d'Orléans, rue Charles Sadron, 45071 Orléans Cédex 02, France, Université d'Orléans, rue de Chartres, 45069 Orléans Cédex 02, France, F. A. Janssens Laboratory of Genetics, Katholieke Universiteit Leuven, K. Mercierlaan 92, B-3001 Heverlee, Belgium, Laboratoire de Biochimie et Technologie des Protéines, INRA, rue de la Géraudière, BP 1627, 44316 Nantes Cédex 05, France, and Jealott's Hill Research Station, Zeneca Agrochemicals, Bracknell Berkshire RG426ET, U.K.

Received September 22, 1997; Revised Manuscript Received December 23, 1997

ABSTRACT: The three-dimensional solution structure of *Ace*-AMP1, an antifungal protein extracted from onion seeds, was determined using ^{1}H NMR spectroscopy and molecular modeling. This cationic protein contains 93 amino acid residues and four disulfide bridges. Its structure was determined from 1260 NOE-derived distance restraints and 173 dihedral restraints derived from NOEs and $^3J_{C_aHNH}$ coupling constants. The global fold involves four helical segments connected by three loops and a C-terminal tail without regular secondary structures, except for a 3_{10}-helix turn and a β-turn. The most striking feature is the absence of any continuous cavity running through the whole molecule as found in recently determined structures of nonspecific transfer proteins extracted from wheat and maize seeds, although their global folds are very similar. Consistent with the absence of a cavity in the core of *Ace*-AMP1, it was found that this protein, in contrast to ns-LTPs, does not bind fluorescently labeled phospholipids in solution. On the other hand, *Ace*-AMP1 is able to interact with phospholipid membranes as shown by the release of carboxyfluorescein from the lumen of artificial liposomes and by the induction of alterations in fluorescence polarization of fluorescently labeled phospholipids embedded in artificial liposomes.

Various antimicrobial proteins have been proposed to be involved in the protection of seeds against potential microbial invaders during their germination on substrates rich in microorganisms. Since the initial discovery of the antimicrobial properties of thionins in 1942 (*1*), other antimicrobial proteins have been isolated from plants such as β-1,3-glucanases (*2*, *3*), permatins (*4*), ribosome-inactivating proteins (*3*, *5*), cysteine-rich antimicrobial peptides (*6*−*8*), plant defensins (*9*−*11*), 2S albumins (*9*, *10*), and several nonspecific lipid transfer proteins (ns-LTPs) (*12*, *13*). Recently, Cammue et al. (*14*) have isolated a protein from onion seeds, named *Ace*-AMP1, which exhibits a higher antimicrobial activity than *Rs*-ns-LTP, a ns-LTP-like protein extracted from radish seeds (*9*). *Ace*-AMP1 is active against numerous fungi at concentrations $\leq 10\ \mu$g/mL, and in contrast to that of *Rs*-ns-LTP, its activity is weakly affected by inorganic cations at physiological concentrations (*14*). *Ace*-AMP1 is synthesized with an N-terminal signal peptide and a C-terminal propeptide of 12 amino acid residues which are both absent from the mature protein. The C-terminal propeptide of *Ace*-AMP1 precursor is rich in hydrophobic and acidic residues as found in C-terminal propeptides of precursors of many vacuolar plant proteins (*15*). Such C-terminal propeptides have often been shown to be determinants for targeting the proteins to the vacuole (*16*, *17*). The subcellular location of *Ace*-AMP1 remains nevertheless to be determined.

Ace-AMP1 is a 93-residue protein, including eight cysteines engaged in four disulfide bridges. The positions of the eight cysteine residues are similar to those found in the sequences of ns-LTPs. A sequence alignment between *Ace*-AMP1 and maize ns-LTP reveals 32% identity and 49% similarity (*18*). On the basis of such sequence similarities, *Ace*-AMP1 could be considered a member of the ns-LTP family. Nevertheless, it does not exhibit the characteristic property of these proteins, i.e., the ability to transfer lipids between membranes of vesicles or organelles in vitro (*14*). The most striking features of the *Ace*-AMP1 sequence are the high percentage of arginine residues (20%) and the presence of a tryptophan doublet in the C-terminal region.

We have previously determined the solution structures of two ns-LTPs extracted from wheat (*19*) and maize seeds (*20*). At the same time, the X-ray structures of maize ns-LTP and its complex with a lipid were determined by Shin et al. (*21*). Recently, the solution structures of a barley ns-LTP (*22*) and

† This work was supported by the Centre National de la Recherche Scientifique (CNRS), the Université d'Orléans, the Région Centre, and the Institut National de la Recherche Agronomique (INRA). It forms part of Séverine Tassin's thesis supported by a Région Centre grant.

* Correspondence should be addressed to Centre de Biophysique Moléculaire, rue Charles Sadron, 45071 Orléans, France. Telephone: (33) 02 38 25 55 74. Fax: (33) 02 38 63 15 17. E-mail: tassin@cnrs-orleans.fr.

‡ Centre de Biophysique Moléculaire (CNRS) et Université d'Orléans.

§ Katholieke Universiteit Leuven.

|| Laboratoire de Biochimie et Technologie des Protéines, INRA.

⊥ Zeneca Agrochemicals.

Université d'Orléans.

S0006-2960(97)02351-9 CCC: $15.00
Published on Web 02/27/1998

its complex with palmitoyl coenzyme A were established from ^{1}H and ^{13}C NMR data (*23*). Similar folds involving four helixes wound in a right-handed superhelix and a C-terminal region devoid of regular secondary elements were found in these three-dimensional structures. The structures of wheat and maize ns-LTPs showed an internal elongated hydrophobic cavity running through the whole molecule (*19*−*21*) which has been shown to be the site for lipid binding (*20*, *21*). More recently, we have proposed a model of the structure of *Ace*-AMP1 by using homology modeling (*18*).

Despite the extensive study of the structure of ns-LTPs using a variety of techniques, a debate is still open on their possible role in vivo. Different functions have been proposed such as playing a role in the formation of cutin by transporting the hydrophobic cutin monomers to the apoplast (*24*) or playing a role as antimicrobial agents in the defense of plants against pathogens (*9*, *13*, *25*).

In this paper, we report on the three-dimensional structure of *Ace*-AMP1 in solution determined on the basis of NMR spectroscopy experiments. This study enables us to point out striking analogies between the global folds of *Ace*-AMP1 and ns-LTPs but also important differences in the organization of their internal cavities which are probably related to their capacity to bind lipids.

MATERIALS AND METHODS

Lipid−*Ace-AMP1 Interaction Studies*. Fluorescence emission spectra of *Ace*-AMP1 were recorded with an Amincon SLM 4800 spectrofluorometer. Excitation and emission wavelengths were set to 295 and 335 nm (slits of 4 nm), respectively. For the titration of proteins with various lipids, the following procedure was used. Two to four microliters of aqueous dispersions of wheat total polar lipids, phospholipids in 10 mM sodium phosphate buffer at pH 7.0 (either 1 or 10 mg/mL), was added stepwise to 1 mL of protein solution (0.1 mg/mL, 8 μM) in the same buffer. After incubation for 1 min, the fluorescence emission spectra were recorded at 20 °C. Fluorescence data were corrected for background signals by using the corresponding lipid solutions alone.

Lipid transfer assay was performed using fluorescent phospholipid probes 1-palmitoyl-2-pyrenyldecanoyl-*sn*-glycero-3-phosphocholine (pyr-PC) and the corresponding phosphoglycerol derivative (pyr-PG) as previously described (*26*, *27*). Lipid binding was tested by adding different ns-LTPs (wheat, maize, and barley) and *Ace*-AMP1 to 1.5 mL of a liposomal suspension of 1 μM pyr-PC or pyr-PG. In the binding assay, the final protein to fluorescent probe molar ratio was about 5. In both fluorescence transfer and binding assays, the excitation wavelength was set to 346 nm (4 nm slit) and the emission wavelength was set to 378 nm (4 nm slit). All measurements were carried out at 25 °C.

The effect of proteins on lipid dynamics was studied by fluorescence polarization of a lipophilic probe, diphenylhexatriene (DPH), embedded within the hydrophobic core of phospholipid bilayers. Excitation and emission wavelengths were set to 360 and 435 nm (band width of 4 nm), respectively. Measurements of the fluorescence intensities detected through polarizers oriented parallel ($I_{||}$) and perpendicular ($I_{\perp}$) to the plane of polarization of the excitation light beam allowed us to calculate the steady state polarization parameter P [$=(I_{||} - I_{\perp})/(I_{||} + I_{\perp})$]. For DPH labeling, 50 μL of a DPH solution (17 μg/mL) diluted in methylene chloride was added to 500 μL of the lipid solution (1 mg/mL, DPH/lipid ratio $\sim$ 1/250). After drying, 1.5 mL of the 10 mM sodium phosphate buffer at pH 7.0 was added and the solution was mixed as described above. One milliliter of a diluted solution in phosphate buffer was poured into a quartz cuvette, and titration was performed by adding stepwise a protein solution (1 mg/mL) in phosphate buffer. The polarization data were recorded before and after the transition temperature of DMPG and DMPC (23 °C) from 15 to 45 °C.

Carboxyfluorescein (CF) release from liposomes was performed according to a modification of the procedure described by Wilschut (*28*). Briefly, a 50 mM solution of HPLC-purified carboxyfluorescein (Molecular Probes) in 5 mM HEPES containing 1 mM EDTA was adjusted to pH 7.4 with 1 N NaOH. Six hundred microliters of this solution was added to 2.3 mg of a dry equimolar mixture of eggPG and eggPC (Sigma-Aldrich) and the mixture vortexed until all the phospholipids were dispersed. This solution was then extruded under high pressure through a 400 nm polycarbonate filter. Large unilamellar vesicles with encapsulated CF were separated from nonencapsulated CF by size exclusion chromatography on a PD-10 (Pharmacia) column eluted with HEPES buffer (5 mM HEPES, 1 mM EDTA, and 100 mM NaCl at pH 7.4). For the CF release assay, the liposome solution was diluted in HEPES buffer so the absorbance would be below 0.2 at 493 nm. The kinetics of CF release were recorded by the fluorescence increase at 520 nm (excitation at 490 nm). One hundred percent release was obtained by lysing vesicles in the presence of 1% Triton X-100.

NMR Experiments. *Ace*-AMP1 was purified from onion (*Allium cepa* L.) seeds as previously described (*14*). The NMR sample was prepared from lyophilized material to make up a 3 mM solution in a mixture of 90% H_2O and 10% D_2O. The pH was subsequently adjusted to 5.0.

All NMR measurements were performed on a Bruker AMX 500 MHz NMR spectrometer equipped with a three-axis field gradient unit. Quadrature detection in the indirectly detected dimensions was performed using the States method (*29*). NMR spectra were processed using the UXNMR program from Bruker on a X32 workstation. The following experiments were carried out at a temperature of 308 K: double-quantum COSY (2Q-COSY) with a mixing time of 30 ms, total correlation spectroscopy (clean-TOCSY) with a 90 ms mixing time performed with a MLEV17 sequence (spin-lock field of approximately 10 kHz) (*30*), purged COSY (P-COSY) (*31*), triple-quantum-filtered COSY (TQF-COSY) (*32*), relayed COSY (*33*) with a 40 ms relay period, and NOESY with a 60 ms mixing time. Additional NOESY experiments with a 200 ms mixing time were carried out at temperatures of 298, 308, and 318 K. In all cases, the water signal was suppressed prior to the free induction decay detection by using the WATERGATE sequence (*34*) in which the selective inversion was achieved through a 3−9−19 composite pulse and an interpulse delay of 250 ms. In TOCSY and COSY experiments, a weak field (approximately 10 Hz) presaturation applied during the relaxation period was followed by a SCUBA sequence (*35*). The measurements

of proton exchange rates were performed at 308 K as follows. The protein sample in H_2O first lyophilized and then dissolved in D_2O at 273 K was placed in a preshimmed spectrometer approximately 15 min after dissolution. Two NOESY spectra were acquired, one short (4 h) and one long (17 h), with a mixing time of 200 ms, which was followed by a TOCSY experiment with a mixing time of 90 ms.

All spectra were recorded with a spectral width of 7052 Hz in both dimensions and 2048 × 650 time domain data points, except for NOESY experiments used for the structure calculations which were acquired with 4096 × 650 data points. Sine bell apodization functions were used prior to Fourier transformation. Application of zero-filling resulted in 2K × 1K data points for all spectra and 4K × 1K real points for NOESY spectra used for structure calculations.

Modeling of the Three-Dimensional Structure. Models of the *Ace*-AMP1 three-dimensional structure in solution were built using the hybrid method of distance geometry and the simulated annealing protocol (*36*) on Silicon Graphics workstations. The assignment of all NOESY cross-peaks was obtained with repeated rounds of structure calculations with DIANA (*37*, *38*) and with ASNO (*39*) software packages. The cross-peak volumes were integrated from the NOESY spectrum recorded with a 60 ms mixing time using EASY (*40*). Peak volumes were translated into upper limit distance restraints using the CALIBA program (*37*, *38*) with an upper distance limit of 5.0 Å for the weakest volumes, and the strongest NH_i-NH_{i+1} connectivity in regular helixes was used as a reference. To take spin diffusion effects into account, cross-peaks appearing on the 200 ms mixing time NOESY spectrum and absent on the 60 ms NOESY spectrum were further considered and converted into a fixed distance of 6.0 Å, irrespective of the cross-peak volume intensity. A first set of structures was generated with DIANA and was used to redefine the 10 calibration classes of the CALIBA program. The final data set consisted of 1260 distance restraints, including 220 intraresidual, 320 sequential, 339 medium-range ($|i - j| \leq 5$), and 378 long-range distance restraints. Sxity-six $^3J_{C_\alpha HNH}$ coupling constants were deduced from the NOESY spectrum using the back Fourier transform procedure of the INFIT program (*41*) and were used together with the distance restraints to generate 76 ϕ, 76 ψ, and 15 χ^1 torsion angle restraints with the HABAS program (*37*). Thirty-six prochiral groups were stereospecifically assigned with the GLOMSA program (*37*). Hydrogen bonds found by DIANA in a majority of structures during the different rounds of calculations were progressively introduced as restraints. They were converted into upper bond distance limits of 3.5 and 2.5 Å and lower bond distance limits of 2.7 and 1.8 Å for CO−N and CO−HN, respectively. To define the four disulfide bridges, distance restraints were added in the following range: 1.9−2.1 Å for $S\gamma(i)-S\gamma(j)$ and 2.5−3.5 Å for $C\beta(i)-S\gamma(j)$ and $C\beta(j)-S\gamma(i)$.

Starting from 200 randomized structures and keeping only unambiguously defined restraints, a first set of conformations was obtained using the DIANA program. The 30 structures with the lowest target function were selected for further calculations using the REDAC strategy (*38*). Additional restraints were incorporated in successive stages according to the concept of structure-aided assignment of ambiguous NOE cross-peaks with the ASNO program (*39*). Each new set of restraints was used as input for a new round of calculation, and this protocol was repeated eight times until all NOESY cross-peaks were assigned.

The 30 structures with lowest target function (TF < 5 Å^2) were then subjected to simulated annealing using the XPLOR 3.1 program (*42*). Subsequently, 15 structures, exhibiting the smallest restraint violations and presenting at least 65% of their (ϕ and ψ) torsional angles in the most favorable region of the Ramachandran map, were minimized using the CHARMM force field (*43*) implemented in XPLOR. The PROMOTIF (*44*) and PROCHECK programs (*45*) were used to analyze and to check the quality of the structures.

RESULTS

Sequence-Specific Assignments

An almost complete sequence-specific assignment of the ^{1}H NMR spectra (Supporting Information) was performed according to the well-established sequential assignment procedure of Wüthrich (*46*), using a combination of COSY, TOCSY, 2Q-COSY, and NOESY two-dimensional experiments recorded at a temperature of 308 K. Due to severe redundancy of some amino acid residues in the primary structure of the protein (19 arginines and 9 prolines), a sequential assignment pathway was also followed on NOESY spectra recorded at 298 and 318 K. The good dispersion of the amide ^{1}H resonances, as shown in Figure 1 where two spectral regions of a NOESY spectrum recorded at 308 K with a 200 ms mixing time are plotted, led to an almost continuous stretch of sequential NOEs over the whole molecule. The only exception concerned the C-terminal region where the assignment of the tripeptide Ile87-Gln88-Cys89 remained very ambiguous due to the high exchange rate of the amide protons and to peak overlapping in the aliphatic proton resonance region. The assignments of the five glycine $C\alpha H_2$ were confirmed through a 2Q-COSY experiment, since the glycine remote connectivities resonated in a typical free spectral region. In addition, this experiment confirmed the degeneracy of $C\alpha H_2$ proton resonances of Gly52. A relayed COSY spectrum recorded at 308 K confirmed the assignments of the $C\beta H$ protons through a relay to amide protons. The nine prolines of *Ace*-AMP1 were all found in the trans configuration characterized by $C\alpha H(i-1)-C\delta H_2(i)$ and $NH(i-1)-C\delta H_2(i)$ NOE connectivities.

Secondary Structures

The amide exchange data and the short- and medium-range dipolar connectivities observed for the backbone protons in a 200 ms NOESY spectrum in H_2O are summarized in Figure 2. The presence of four helical secondary structure elements is first derived from a dense array of characteristic NOEs and from stretches of slowly exchanging backbone amide protons. Successive rounds of calculations led us to define more accurately the extent of the four α-helixes encompassing residues Cys4−Leu19 (H1), Ala25−Leu34 (H2), Leu42−Asn57 (H3), and Arg65−Arg74 (H4). Most hydrogen bonds characterizing these helixes are present in a majority of selected structures and are all supported by slow NH ^{1}H−^{2}H exchange rates and by low values of $^3J_{C_\alpha HNH}$ coupling constants (Figure 2). The only discrepancy is found for the coupling constants of some residues in the H4 helix which

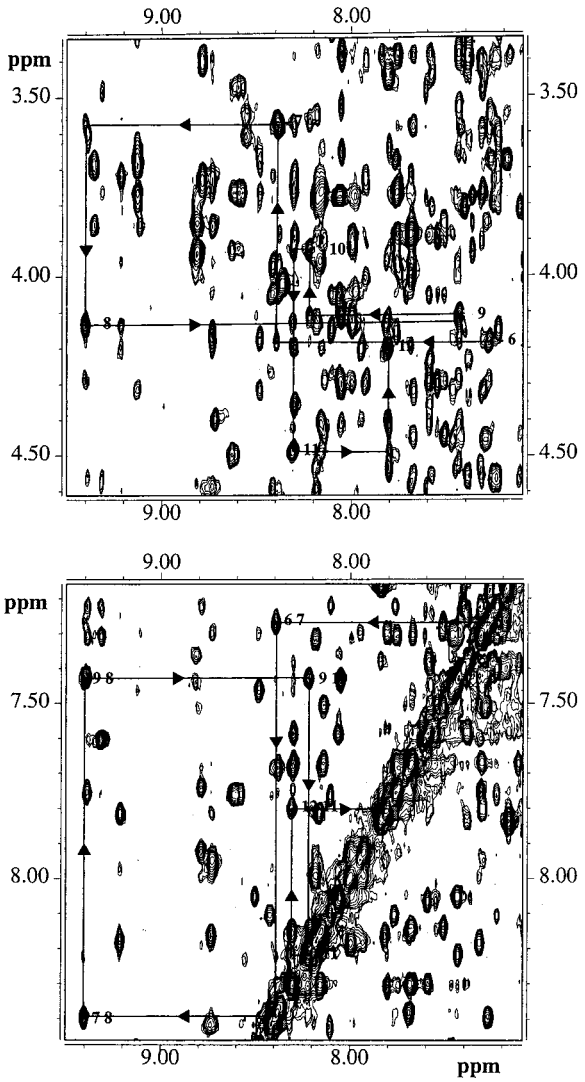

FIGURE 1: Two spectral regions of a NOESY spectrum of *Ace*-AMP1 in 9/1 H_2O/D_2O at 308 K with a 200 ms mixing time and the assignment pathway for the first helix from residue 6 to 12.

starts after a proline residue (Pro64) and which contains a proline residue (Pro70) in the middle of its sequence (see below). The Asn75−Asn93 fragment includes extended conformations and two well-organized fragments: a 3_{10}-helix turn (Val78−Phe81) and a β-turn (Arg84−Ile87).

Disulfide Bridges

The three-dimensional structure of *Ace*-AMP1 is stabilized by four disulfide bridges (*14*). In the absence of chemical characterization, these covalent links were determined according to the following procedure. The distance between the Hβ protons of one Cys residue and the Hα proton of the second one engaged in the same disulfide bridge is in a range in which NOEs can be theoretically detected (*47*). Nevertheless, local dynamics or a special conformation can strongly reduce these NOEs, thus hampering their detection. Several inter-cysteine NOE connectivities allowed us to identify clearly two disulfide bridges: Cys14−Cys27 and Cys28−Cys73 (Table 1). Since in the Cys4−Cys49 bridge the β-proton resonances of the two cysteine residues almost overlap, inter-residue connectivities could not be unambiguously assigned. This bridge was deduced indirectly via long-range connectivities between Cys49 and Val7 or Asn8 residues which are adjacent to Cys4 in the H1 helix. The only possibility for the last bridge was Cys47−Cys89 even if any Cys89 proton resonances could be identified. The proposed disulfide pairings, Cys4−Cys49, Cys14−Cys27, Cys28−Cys73, and Cys47−Cys89, are fully compatible with the distance restraints (Table 2) and with the disulfide pattern found for all known ns-LTP structures (*19*−*22*).

Three-Dimensional Structure

Quality of the Structure. Table 2 gives an evaluation of the quality and precision of the structures determined from NMR data. In the 15 selected structures, there is no structure with distance violations larger than 0.4 Å and the average number of violations larger than 0.3 Å is only 0.2. Considering the number of NOEs per residue (Figure 3), the secondary structure elements are particularly well-defined, in contrast with the loop and turn regions where some variability is observed. In the four helixes H1−H4, the average pairwise root-mean-square deviations (rmsds) are 0.62 Å for the backbone atoms (N, Cα, and C′) and 1.13 Å for all heavy atoms. These values drop to 0.44 and 0.97 Å, respectively, when the rmsds are calculated with respect to the average structure. The highest rmsd values are confined to the loops connecting the helixes and to the very end of the C-terminal region (Figure 3). All these values are typical of high-resolution NMR structures. An efficient assessment of the structure quality may be obtained from the distribution of the residues in a (ϕ vs ψ) Ramachandran plot (*48*). PROCHECK concludes that 70% of the (ϕ and ψ) pairs of the 15 minimized structures of *Ace*-AMP1 lie within the most energetically allowed regions and 29% in the extended favorable regions.

Global Fold. The global fold of *Ace*-AMP1 shown in Figure 4 is stabilized by four disulfide bonds and involves four amphipatic helixes (H1−H4) and a C-terminal segment defined above. As in all ns-LTP structures, the Pro13 residue produces a break in the hydrogen bond network of helix H1 and induces a kink of about 20°. A PROCHECK analysis of the 15 best structures showed that the H2 helix (residues 25−34) ends up at residue Leu34 and displays a characteristic α-helical hydrogen bond pattern. The two next residues, Arg35 ($\phi = -30.5°$ and $\psi = -32.3°$; ϕ and ψ averaged over the 15 structures) and Phe36 ($\phi = -76.3°$ and $\psi = -24.9°$), are located in the helical regions of the Ramachandran map, but they are not involved in regular hydrogen bonds with the preceding residues. The N terminus of helix H2 is connected to helixes H1 and H4 through two disulfide bridges, Cys27−Cys14 and Cys28−Cys73. The third helix H3 (residues 42−57) is interrupted by a proline residue (Pro58). However, in 10 out of the 15 selected structures, the three residues following Pro58 are involved in a supplementary α-helical turn (residues 59−62) stabilized by a hydrogen bond between the carbonyl of Pro58 and the amide proton of Arg62. The NH proton of Leu60 was found to exchange slowly, and in all structures, this fragment is linked to the H3 helix by a hydrogen bond with the carbonyl of Asn57. The Pro58 residue induces a severe kink of about 90° between helix H3 (residues 42−57) and the supplementary α-helical turn (residues 59−62). As is often observed in distorted helixes of ns-LTPs, high $^3J_{CahNH}$ coupling constants are found for the residues preceding prolines (8.2

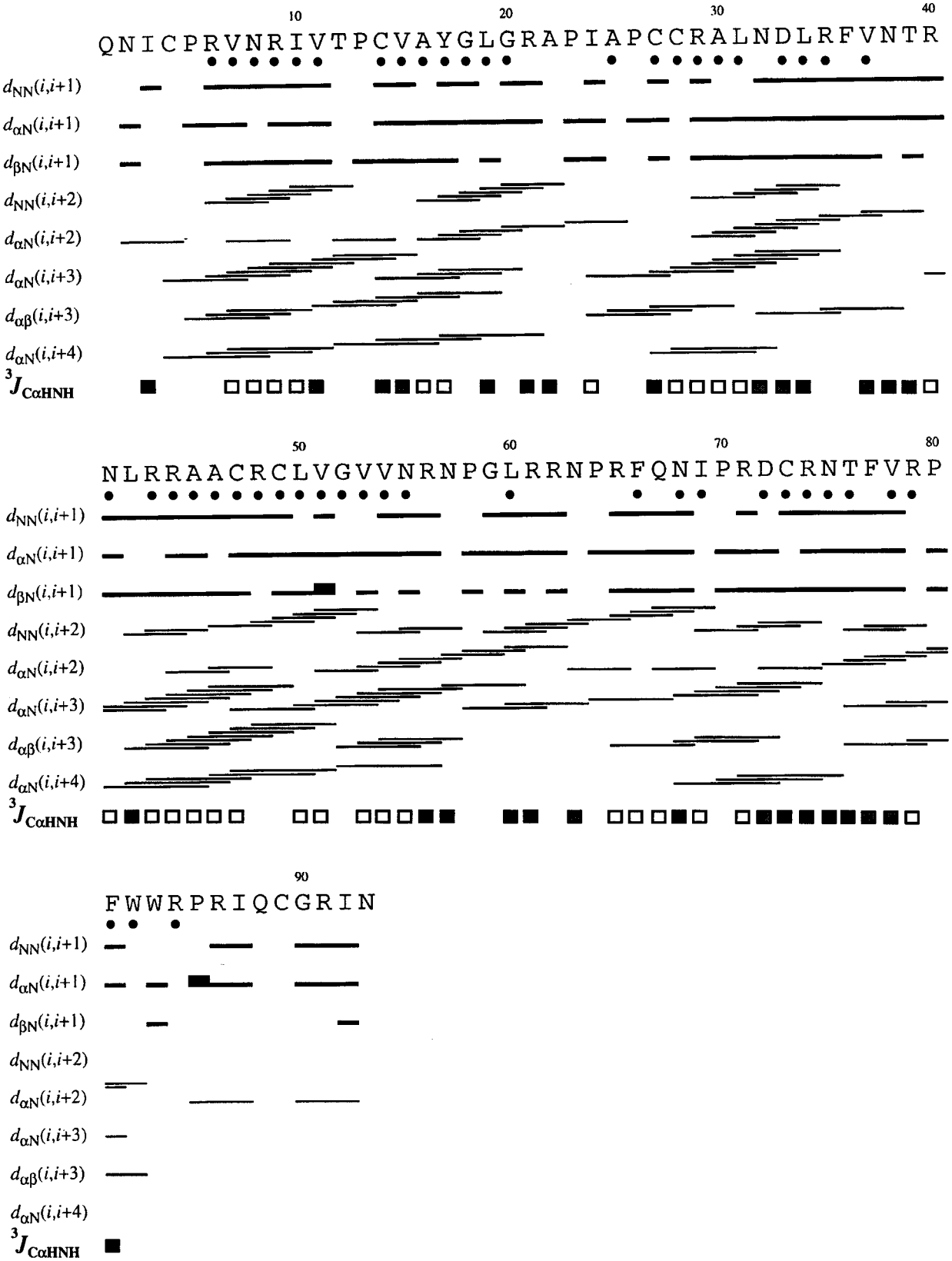

FIGURE 2: Summary of the data on the sequentials NOE, slow amide proton exchange rates (marked with a ●), and $^3J_{C_\alpha HNH}$ coupling constants (black for $^3J_{C_\alpha HNH} > 8$ Hz, gray for 6 Hz $< {}^3J_{C_\alpha HNH} > 8$ Hz, and white for $^3J_{C_\alpha HNH} < 6$ Hz) determined by NMR for *Ace*-AMP1.

and 10.8 Hz for Arg56 and Asn57, respectively). The H3 helix is linked to helix H1 and the C-terminal segment through two disulfide bridges, Cys4−Cys49 and Cys47−Cys89. The last helix, H4, is preceded by a γ-turn stabilized by a hydrogen bond between the carbonyl of Asn63 and the amide proton of Arg65. In this helix, including residues 65−74, the hydrogen bond network is somewhat irregular showing both 3_{10}- and α-helical characteristics as previously observed for the wheat ns-LTP structure (*19*). These irregularities arise from the presence of two proline residues,

Table 1: NOE Connectivities Defining the Disulfide Pairings

disulfide bridge	inter-residue NOE connectivity	
Cys4−Cys49	QG1 Val7	HB2 Cys49
	QG1 Val7	HB3 Cys49
	QG2 Val7	HB2 Cys49
	QG2 Val7	HB3 Cys49
	HB2 Asn8	HA Cys49
Cys14−Cys27	HA Cys14	HB3 Cys27
	QB Cys14	HB2 Cys27
	HA Cys14	HN Cys27
	HN Cys14	HB3 Cys27
	HN Cys14	HB2 Cys27
Cys28−Cys73	HA Cys28	HB2 Cys73

Table 2: Structural Statistics of the 15 Best Structures of *Ace*-AMP1

	mean number	min, max
Mean Number of Violations of Experimental Restraints		
distance restraints of >0.3 Å	0.20	0, 1
distance restraints of >0.2 Å	1.40	0, 3
angle restraints of >10 °	4.46	2, 7
Deviation from Idealized Geometry		
bond distances of >0.05 Å	5.80	4, 9
angles of >10°	4.00	2, 9
Ramachandran		
most favorable regions	70%	72, 65
additional regions	29%	31, 26

	rmsd from the average structure (Å)	pairwise rmsd (Å)
backbone (1−93)	1.11 ± 0.17	1.61 ± 0.41
helixes	0.44 ± 0.04	0.62 ± 0.08
H1 (4−19)	0.31 ± 0.07	0.45 ± 0.10
H2 (25−34)	0.29 ± 0.09	0.41 ± 0.15
H3 (42−57)	0.30 ± 0.07	0.36 ± 0.09
H4 (65−74)	0.18 ± 0.07	0.23 ± 0.08
C-terminal region (75−93)	1.26 ± 0.36	1.78 ± 0.75

Pro64 and Pro70. The C-terminal segment (residues 75−93) contains one 3_{10}-helical turn (residues 78−81) and a β-turn (residues 84−87). Its first part is packed against the H4 helix, whereas its last part is approximately parallel to the H3 helix.

Disulfide Bridges and Side Chains. The conformations adopted by the four disulfide bridges are reported in Table 3. The Cys28−Cys73 bridge experiences two equally populated conformations, whereas the Cys14−Cys27 one adopts one well-defined conformation. Conversely, the ill experimental definition of Cys4 and Cys89 residues leads to variable conformations of the Cys4−Cys49 and Cys47−Cys89 bridges. All cysteines but Cys89 adopt staggered orientations around the $C_\alpha-C_\beta$ bond, and Cys14, Cys47, and Cys49 residues are well-defined ($\chi^1 < 0.1$) (Figure 3). Moreover, for the first three disulfide bridges, Cys4−Cys49, Cys14−Cys27, and Cys28−Cys73, χ^{SS} angles are very close to the expected values for energetically favorable conformers, i.e., ±90° (*49*).

Most side chain conformations are well-defined since 63% of the χ^1 circular variances are lower than 0.1 (Figure 3). The 19 arginine residues distributed over the sequence of *Ace*-AMP1 are all exposed to the solvent, and therefore, most of their side chains are badly defined. Only Arg44, Arg65, Arg79, and Arg84 side chains have χ^1 circular variances lower than 0.1 (Figure 3). Some of them are involved in hydrogen bonds or salt bridges. For instance, the side chain guanidinium groups of Arg43 and Arg44 form a hydrogen bond with the C-terminal group. This hydrogen bond can be related to the low-field chemical shift of the ϵNH proton of Arg43 (9.3 ppm). In 9 refined structures, the guanidinium group of Arg65 is quite close to the oxygen of the hydroxyl of Tyr17 (2.8 Å). In the TOCSY cross-peak pattern of the aromatic ring, the Hδ protons are coupled to two nonequivalent protons and give rise to two very broad cross-peaks. At 35 °C, their line width is almost 100 Hz. Increasing the temperature to 45 °C leads to an increase of the line width of up to 150 Hz of the most downfield located cross-peak, while the intensity of the second one is drastically reduced. These observations are in agreement with a restricted mobility of the Tyr17 side chain, most probably due to a hydrogen bond. In most structures, the side chain of Arg79 points toward the hydroxyl oxygen of Thr76. However, a hydrogen bond is found in only 6 structures among 15. Finally, in 7 out of 15 structures, the guanidinium group of Arg86 is involved in a hydrogen bond with the side chain carbonyl of Asn55 (2.8 Å). *Ace*-AMP1 contains two acidic residues, Asp33 and Asp72, which belong to the H2 and H4 helixes, respectively, and whose side chains are well-defined. Asp33 appears to be involved in a salt bridge with the guanidinium group of Arg6, as shown in 7 out of 15 structures.

Hydrophobic Core. The hydrophobic aliphatic residues of the four amphipatic helixes (Val7, Ile10, Val11, and Val15 in helix H1, Ile24, Leu31, Leu34, and Val37 in H2, Leu50, Val51, Val53, and Val54 in H3, and Ile69 in H4) are pointing toward the interior of the protein, generating a large and extended hydrophobic core. Unlike ns-LTPs, *Ace*-AMP1 contains 7 aromatic residues which are almost all located in the last helix and the C-terminal region. As shown in the superposition of the 15 structures represented in Figure 5, the conformations of aromatic residues are very well defined. All their side chains strongly interact with their near environment and display very well defined conformations as revealed by their χ^1 circular variances which are always lower than 0.01 (Figure 3). The aromatic side chain of Tyr17, belonging to the first helix, is located between the last turn of H1 and the first turn of H2, thus facing residues Ile24 and Ile69. These three amino acids make a partially solvent-exposed hydrophobic cluster at the top of H1. The Phe36 residue located in the last turn of H2 belongs to another hydrophobic cluster involving residues Ile3, Val7, and Leu34, which is partially exposed to the solvent. Phe66, which belongs to the last helix, is oriented toward the core of the protein, makes several contacts with H1, H4, and the C-terminal region, and is included in an aromatic cluster involving residues Trp82 and Trp83. The C-terminal segment contains four aromatic residues, namely Phe77, Phe81, Trp82, and Trp83. The last three residues of this segment belong to the hydrophobic core, while Phe77 is solvent-exposed. Phe81 is in van der Waals contact with the H1 and H2 helixes and is buried in a small hydrophobic cluster involving residues Leu34 and Val37. The Trp82 residue makes contacts with helixes H1, H2, and H4, while Trp83 interacts with helixes H3 and H4 through residues Val51, Val54, and Leu60. Trp82, Trp83, and Phe66 constitute an

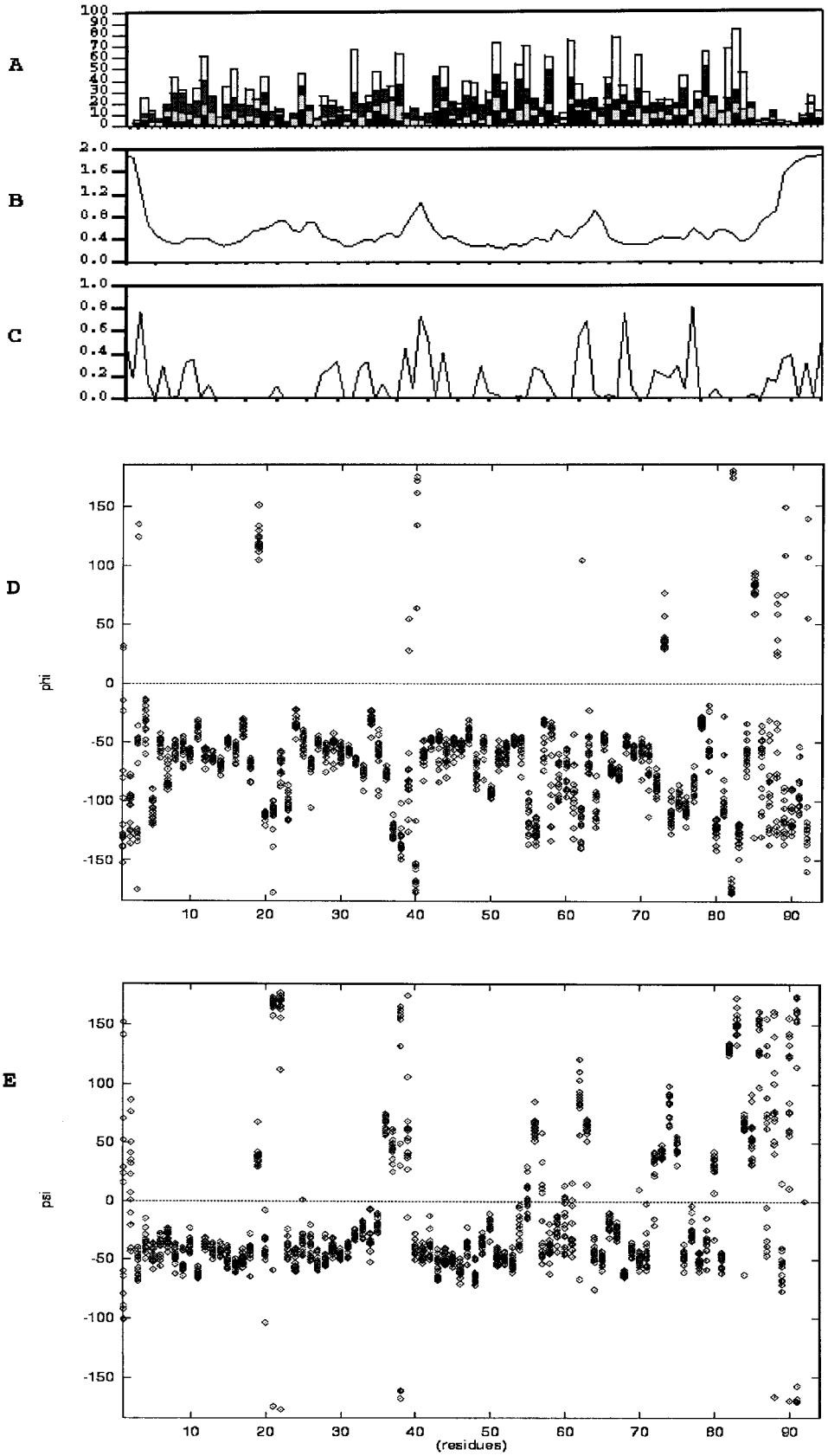

FIGURE 3: Data for the 15 best NMR structures of *Ace*-AMP1 plotted as a function of sequence. (A) Distribution of intraresidual (black), sequential (gray), medium-range (black gray), and long-range (light gray) NOEs by residue. (B) Average local rmsd for backbone atoms (N, Cα, C, and O) for residues 1−93. (C) Distribution of the χ^1 circular variance by residue. The χ^1 circular variance was calculated by PROCHECK (*45*). (D) Distribution of the ϕ angle by residue. (E) Distribution of the ψ angle by residue.

aromatic cluster embedded in the hydrophobic core of the protein. In all structures, the Trp82 side chain facing the Phe66 aromatic ring is not accessible to the solvent. Its indolic proton is involved in a hydrogen bond with the

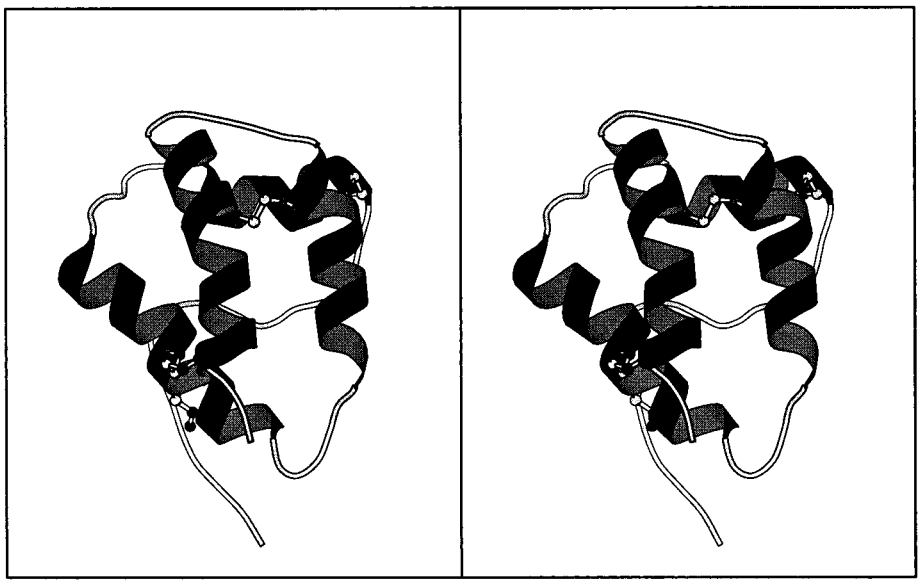

FIGURE 4: MOLSCRIPT (*58*) stereoview of *Ace*-AMP1. Helixes H1 (4−19), H2 (25−36), H3 (42−57), and H4 (65−74) and the four disulfide bridges are reported.

Table 3: Side Chain Dihedral Angles for the Four Disulfide Bridges

	χ^1	χ^2	χ^{SS}	$\chi^{2'}$	$\chi^{1'}$
4−49 (14 structures)	−103.2° (31.8°)	9.5° (40.0°)	−101.3° (18.1°)	−83.5° (11.8°)	−33.7° (12.8°)
14−27 (12 structures)	−87.4° (29.0°)	−82.1° (46.7°)	−89.6° (3.3°)	−38.8° (19.6°)	−54.4° (5.1°)
(3 structures)	−162.5° (2.7°)	73.8° (2.7°)	100.2° (3.7°)	−96.1° (1.6°)	−64.3° (4.5°)
28−73 (8 structures)	−159.3° (29.0°)	−93.3° (18.7°)	−94.8° (17.1°)	−131.8° (6.8°)	−114.0° (15.9°)
(6 structures)	−87.9° (16.9°)	−82.7° (23.9°)	121.4° (3.9°)	119.9° (10.3°)	−102.3° (11.8°)
47−89 (15 structures)	166.6° (8.3°)	−36.4° (117.7°)	−26.7° (109.9°)	77.5° (75.1°)	−91.1° (56.1°)

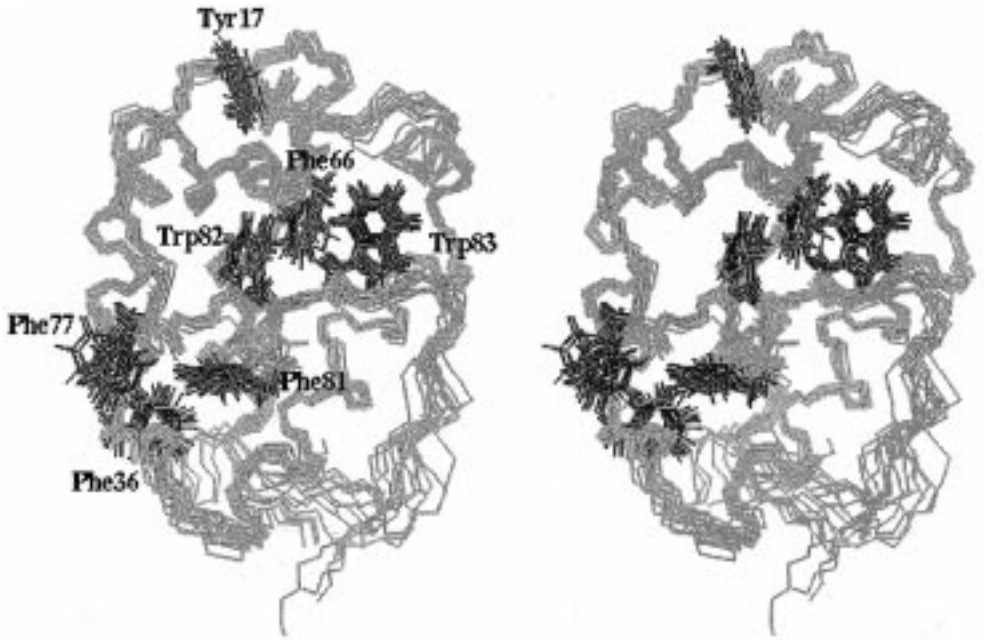

FIGURE 5: Stereoview of the 15 best NMR structures of *Ace*-AMP1 showing the aromatic residues and the polypeptide backbone. The structures are fitted to the Cα atoms of the four helixes.

backbone carbonyl of Phe66 and does not exchange with ^{2}H over a period of several weeks.

Interactions with Phospholipids

The possible interaction of *Ace*-AMP1 with phospholipids was assessed using three different assays. The ability of the protein to bind individual fluorescent pyrene-conjugated phospholipids was first tested. It was found that *Ace*-AMP1 did not induce a change in fluorescence of either pyr-PC or pyr-PG, while the fluorescence of both molecules increased significantly in the presence of wheat ns-LTP (Figure 6a). This result indicates that *Ace*-AMP1, in contrast with wheat ns-LTP, cannot associate with individual phospholipids in solution. A second assay was used to measure the release

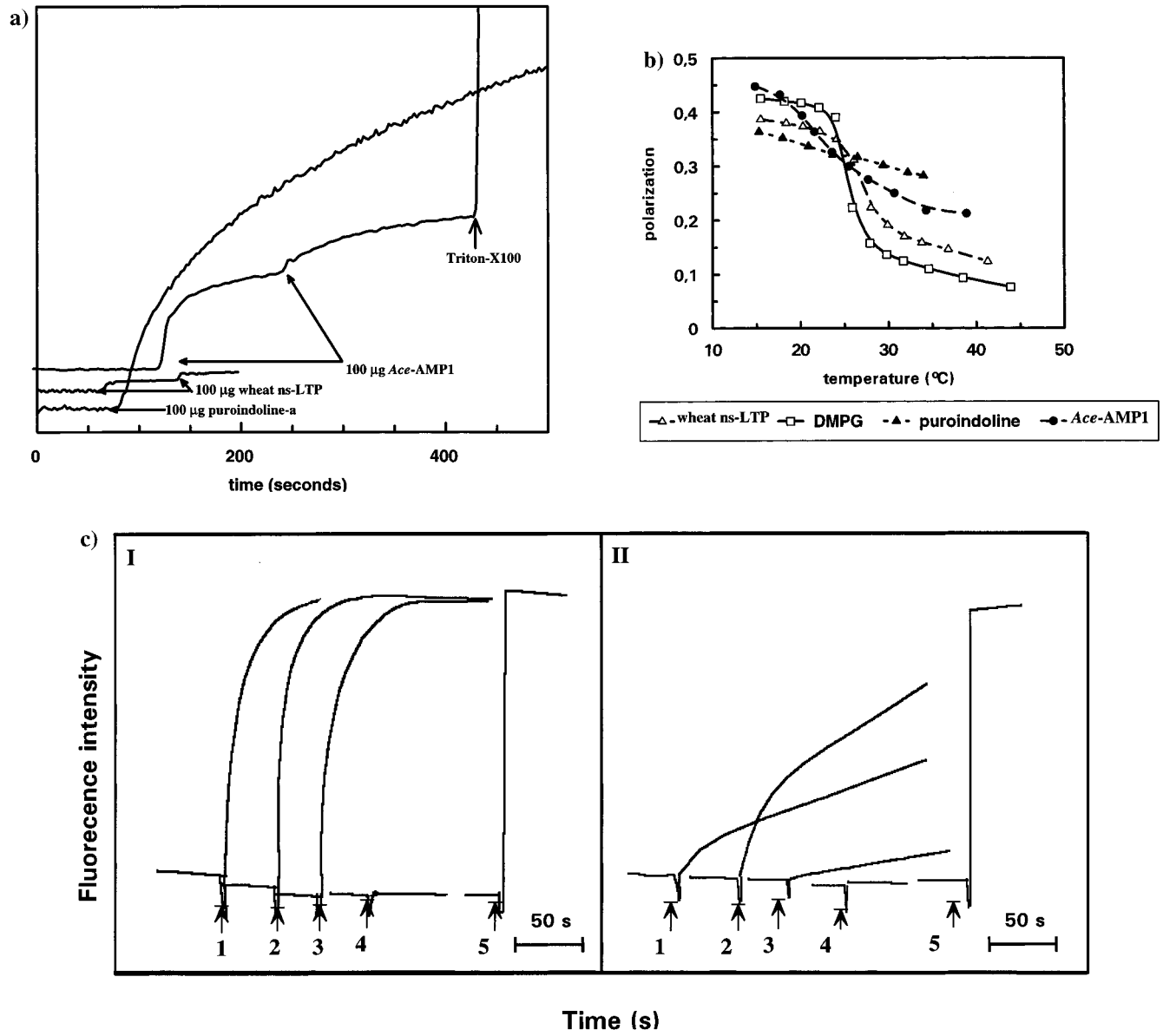

FIGURE 6: (a) Carboxyfluorescein release from liposomes consisting of a PG/PC mixture, induced by *Ace*-AMP1, wheat ns-LTP, and puroidoline-a. Arrows indicated the time of addition of the protein. (b) Fluorescence polarization of the hydrophobic probe, diphenylhexatriene, on gel−fluid liquid-crystalline phase transition of DMPG liposomes. (c) Binding of fluorescent pyr-PG (I) and pyr-PC (II) probes to wheat (1), maize (2), barley ns-LTPs (3), and *Ace*-AMP1 (4). Total fluorescence was measured by adding Triton X-100 (5).

of carboxyfluorescein entrapped in artificial liposomes composed of an equimolar mixture of PG and PC. *Ace*-AMP1 was found to release carboxyfluorescein from such liposomes, indicating that it somehow interacts with the lipid bilayers (Figure 6a). In contrast, wheat ns-LTP was not active in this assay. This release of carboxyfluorescein caused by *Ace*-AMP1 was substantially weaker than that induced by puroindoline-a, a wheat protein known to interact strongly with bilayer vesicles (*50*) (Figure 6a). Finally, a last assay was set up which consisted of measuring fluorescence polarization of a lipophilic fluorescent probe embedded in acidic DMPG bilayer vesicles before and after addition of the protein. *Ace*-AMP1 caused a decrease in cooperativity of the gel to fluid transition (Figure 6b). These effects were observed only when the amount of protein added was high (lipid/protein ratio $R_i = 1-2$), and in contrast with that of puroindoline-a, the phase transition was not suppressed. A slight but significant increase in the transition temperature was observed with wheat ns-LTP with no major changes of transition cooperativity. No effects on the gel−fluid phase transition of neutral DMPC were observed for both wheat ns-LTP and *Ace*-AMP1. The pyrene fluorescence assay was also performed without addition of the acceptor liposomes in order to probe lipid binding. Under these conditions, the protein/lipid molar ratio was 5/1. No fluorescence increase was observed when *Ace*-AMP1 was added to pyr-PG liposomes, contrary to what was observed for wheat, barley, and maize ns-LTPs. Similar results are obtained with pyr-PC (Figure 6c). It was noteworthy that the binding of PC is not immediate, unlike that of pyr-PG. This result was probably due to a difference in the kinetics of the adsorption of protein to the bilayer interface. This adsorption was probably improved by the electrostatic interactions between basic ns-LTP and anionic PG. This experiment showed unambiguously that *Ace*-AMP1 was unable to bind diacylphospholipids, unlike the other cereal ns-LTPs. However, these results do not preclude the binding of monoacylated derivatives to *Ace*-AMP1.

DISCUSSION

Comparison of the Structure of Ace-AMP1 with ns-LTP Structures. *Ace*-AMP1 shares about 32% sequence identity and about 46% sequence similarity with maize ns-LTP. These numbers fall when other ns-LTP sequences are considered (Figure 7). Nevertheless, a superposition of the global folds of *Ace*-AMP1 and wheat (*19*), maize (*20*), and barley (*22*) ns-LTP solution structures reveals striking structural analogies (Figure 8). In the four proteins, the tertiary fold maintained by four disulfide bridges involves four helixes wound on a right-handed superhelix and an extended C-terminal region. Superposition of the experimental structure of *Ace*-AMP1 in solution with that predicted by homology modeling (*18*) reveals the same global fold (Figure 8). The main difference is in the presence of supplementary turns in the structure in solution (residues 59−62 and 79−81) and in the position of some aromatic side chains (Trp82 and Trp83).

The doublet Pro13−Cys14 of the H1 helix is present in the four protein sequences, and the proline residue induces a kink of about 20° in their H1 helix. This kink is associated with high $^3J_{C_aHNH}$ coupling constants in sequence positions $i - 2$ and $i + 1$, where i represents the proline sequence index. Comparison of the average interhelix angles in reported ns-LTP structures and *Ace*-AMP1 (Table 4) shows that the first three helixes have the same directions in all four proteins, forming an up−down−up motif. The main difference between *Ace*-AMP1 and the ns-LTPs seems to be located in the spatial position of helix H4. The precision of the three interhelix angles involving H4 is rather poor for *Ace*-AMP1 structures, due to its 3_{10}- and α-helical mixed characteristics. Another difference between ns-LTPs and *Ace*-AMP1 is the presence in the last protein of one supplementary α-helix turn involving residues Gly59−Asn62 following the H3 helix and another one involving residues Arg79−Phe81 following the H4 helix. The latter turn seems to be correlated with the insertion of two amino acids, Val78 and Arg79 in *Ace*-AMP1, which are not in ns-LTPs. Val78 and Phe81 belong to the hydrophobic core and are pointing toward the interior of the protein, while Arg79 is oriented outward into the solvent.

In addition to the eight cysteine residues, several hydrophobic residues, namely Val7, Val11, Pro13, Val15, Leu31, Leu34, Val37, Ala46, Leu50, Leu60, Ile69, and Pro80, are conserved between *Ace*-AMP1 and ns-LTP sequences. They are spread all over the different structural elements, and they interact to form the hydrophobic cluster in the core of the protein and therefore contribute to the stability of the protein scaffold. An aromatic residue, Tyr or Phe, is present in all ns-LTPs and in *Ace*-AMP1 at position 17 (*Ace*-AMP1 numbering). In *Ace*-AMP1, a hydrogen bond is found between the Tyr17 and Arg65 side chains. In the maize ns-LTP X-ray structure, such a hydrogen bond would exist considering that the Tyr17 hydroxyl hydrogen is close enough to the oxygen side chain of Asn64. A close analysis of the 13 ns-LTP sequence alignments shows that a lysine or an asparagine residue is present in position 65 in 8 sequences. This observation probably indicates that the hydrogen bond involving Tyr17 is a general feature of ns-LTP structures. The Leu42 residue of *Ace*-AMP1 interacting with Ile3 and Val37 is replaced by an aspartic residue in all ns-LTP sequences. In the maize ns-LTP structure, this aspartic residue is engaged in a salt bridge with the amino group of the N-terminal residue. Different kinds of interactions seems then to be involved in the stabilization of the N-terminal fragment.

A fragment of 8 amino acids involving residues Arg43-Arg44-Ala45-Ala46-Cys47-Xaa48-Cys49-Leu50 is strictly conserved between the maize ns-LTP and *Ace*-AMP1 sequences (Figure 7). Similar interactions are found between Arg43-Arg44 residues and the C-terminal group in *Ace*-AMP1 and Arg45-Arg46 residues and the C terminus in maize ns-LTP. An aromatic residue is present in most ns-LTP sequences at position 81. In maize ns-LTP, this residue (a tyrosine) juts into the protein hydrophobic cavity, thus capping the channel. In the lipid−protein complex (*20*, *21*), this residue participates in the stabilization of the complex via a hydrogen bond between its OH and the lipid carbonyl. In *Ace*-AMP1, this residue is replaced by a phenylalanine and its aromatic ring is in the same location as the tyrosine ring in reported solution structures of ns-LTPs. In the maize ns-LTP X-ray structure, the H3 helix interacts with the second part of the C-terminal region through a hydrogen bond between Lys54 and Thr87 residues (*21*). Such hydrogen bonding is not systematically found in all NMR structures of *Ace*-AMP1 (7 of the 15 structures), indicating that other kinds of interactions could be involved in this region.

A striking structural feature of all known structures of ns-LTP is an internal hydrophobic cavity running through the whole molecule (*19*−*22*). It is first parallel to H1 and then to H4 and is large enough to accommodate one or two aliphatic chains of a lipid (*20*, *21*, *51*). The volume of this cavity can vary from 240 to 500 Å^3 in the maize ns-LTP solution structure without noticeable changes of the overall protein structure (*20*). Slight variations of the C-terminal fragment and side chain conformations of the residues which delineate the cavity lead to such large volume variations. We have recently shown that wheat ns-LTP can form a stable complex in solution with DMPG, a diacylphospholipid (*51*). The calculated structure derived from NOE data revealed that the insertion of the lipid into the hydrophobic cavity did not entail significant changes in the protein structure architecture. The most glaring divergence between the protein and the complex concerns the position of the C-terminal tail which is pushed outward into the solvent. Therefore, it appears that this C-terminal segment can act as a molecular cover capping the hydrophobic crevice delineated by the four helixes and modulating the accessible volume. This peculiarity may explain why these proteins are not specific and are able to transfer different hydrophobic compounds. Although most assays designed to assess the biological activity of ns-LTPs are based on the interaction with phospholipids, the natural ligands of these proteins are actually unknown. To detect the presence of such a cavity in *Ace*-AMP1 solution structures, we have applied the program CAVITE (*18*) which probes and delineates cavities inside protein structures. As shown in Figure 9, *Ace*-AMP1 possesses some sparse and small cavities, but there is no continuous channel as described in ns-LTP structures, although hydrophobic residues which outline the maize ns-LTP hydrophobic pocket are mostly conserved in the sequence of *Ace*-AMP1. This structural difference arises

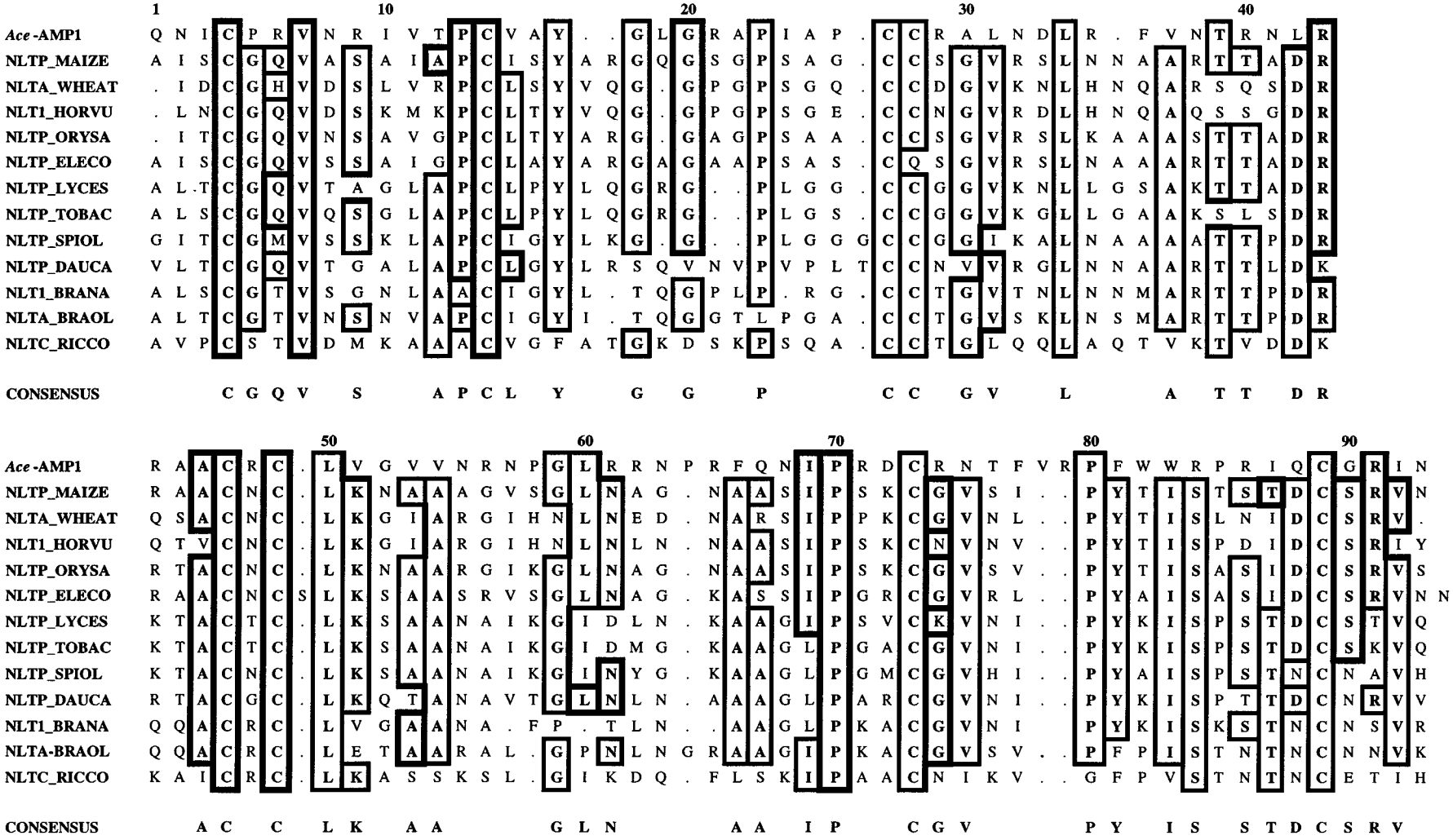

FIGURE 7: Amino acid sequence alignment of 13 different plant ns-LTPs, including *Ace*-AMP1, maize ns-LTP from *Zea maize* seeds (*59*) (Swissprot code NLTP_MAIZE), wheat ns-LTP from *Tricium aestivum* seeds (*60*) (NLTA_WHEAT), barley ns-LTP from *Hordeum vulgare* seeds (*61*) (NLT1_HORVU), rice ns-LTP from *Oryza sativa* seeds (*62*) (NTLP_ORYSA), Indian finger millet ns-LTP from *Eleusine coracana* seeds (*63*) (NTLP_ELECO), tomato ns-LTP from *Lycopersicon esculentum* seeds (*64*) (NLTP_LYCES), tobacco ns-LTP from *Nicotiana tabacum* flowers (*65*) (NLTP_TOBAC), spinach ns-LTP from *Spinacia oleraceae* leaves (*66*) (NLTP_SPIOL), carrot ns-LTP from *Daucus carota* (*24*) (NLTP_DAUCA), ns-LTP from *Brassica napus* (*67*) (NLT1_BRANA), ns-LTP from *Brassica oleracea* (*68*) (NLTA_BRAOL), and castor bean ns-LTP from *Ricinus communis* seeds (*69*) (NLTC_RICO). The bottom line indicates the consensus sequence.

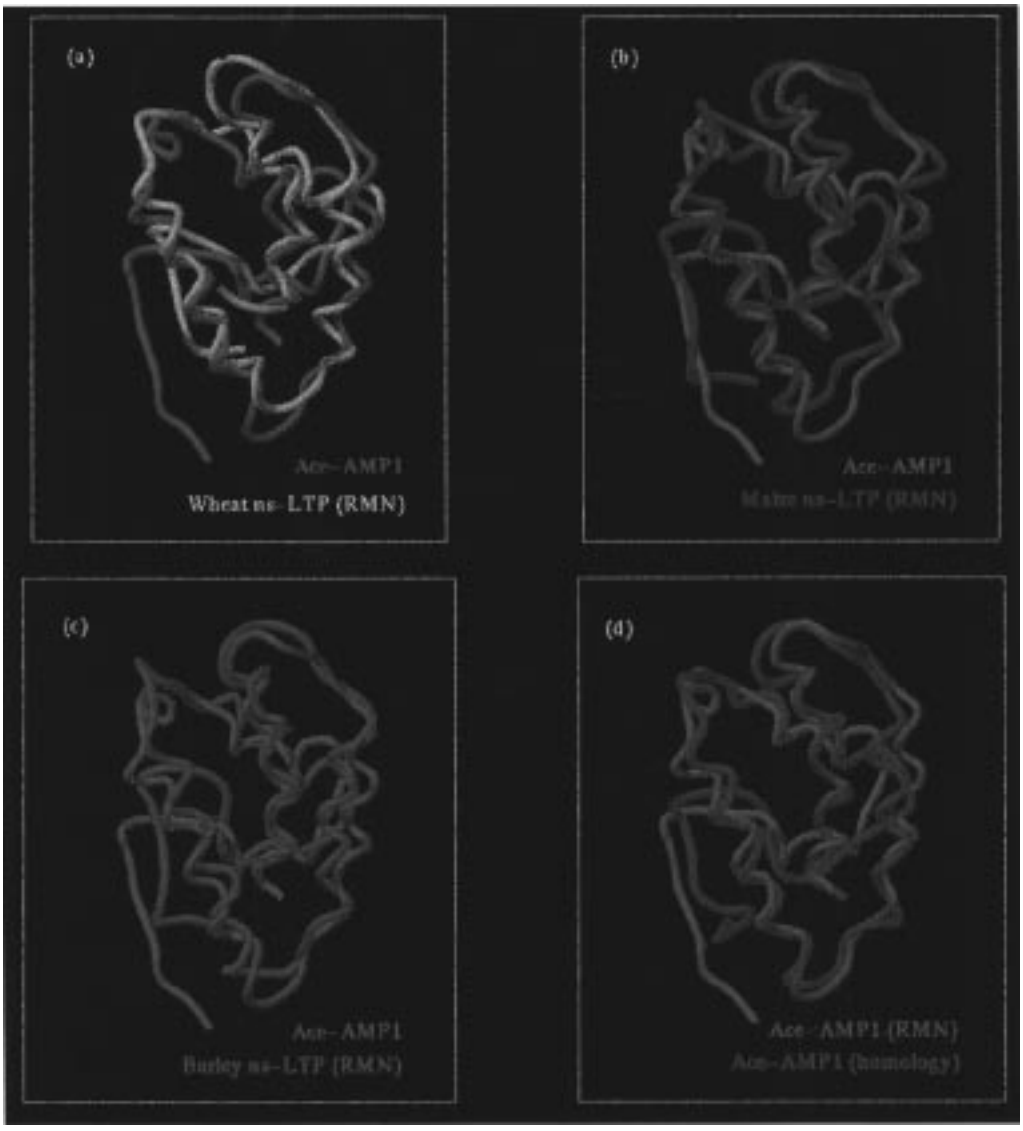

FIGURE 8: Comparison of the *Ace*-AMP1 global fold with that of ns-LTPs. (a) Superposition of *Ace*-AMP1 (magenta) with wheat ns-LTP (yellow) (*19*). (b) Superposition of *Ace*-AMP1 (magenta) with maize ns-LTP (green) (*20*). (c) Superposition of *Ace*-AMP1 (magenta) with barley ns-LTP (blue) (*22*). (d) Superposition of *Ace*-AMP1 (magenta) with *Ace*-AMP1 as determined by homology modeling (green-blue) (*18*).

Table 4: Average Interhelix Angles in Maize, Wheat, and Barley ns-LTPs and *Ace*-AMP1 Structures

helixes	maize ns-LTP	wheat ns-LTP	barley ns-LTP	*Ace*-AMP1
2−1	−146	−143	−146	−142
3−1	−31	−22	−24	−33
3−2	−141	−143	−144	−145
4−1	124	132	123	80
4−2	−78	−72	−64	−86
4−3	140	145	150	108

from the presence of bulky residues Phe66, Trp82, and Trp83 which are found only in the *Ace*-AMP1 sequence. This is shown in Figure 10 where the side chains of these three aromatic residues are displayed within the hydrophobic cavity of maize ns-LTP, whose structure was fitted on the Cα coordinates of *Ace*-AMP1. Actually, the aromatic rings of residues Phe66 and Trp82 are oriented toward the interior of the protein obstructing the channel. The position of the tryptophan residues in the hydrophobic core of the protein is consistent with fluorescence data. The emission peak around 330 nm (result not shown) is close to the emission of a tryptophan in a hydrophobic environment. The absence of any continuous cavity inside the protein structure may be related to its incapacity to transfer lipids between membranes in vitro and to bind diacylphospholipids. However, the two solution structures of complexes of barley ns-LTP−palmitoylCoA (*23*) and wheat ns-LTP−DMPG (*51*) showed that insertion of bulky lipids induces structural rearrangement of the protein structure. In the case of barley ns-LTP, a significant swelling of the structure was observed. In the DMPG complex, the only noticeable difference between the free and complexed structures was a movement of the C-terminal region. According to these observations, we cannot completely exclude the possibility of a structural change of *Ace*-AMP1 taking place upon interaction with lipidic membranes.

Interactions of Ace-AMP1 with Lipids. The different studies performed to evaluate the ability of *Ace*-AMP1 to interact with phospholipids show unambiguously that, in contrast with other plant ns-LTPs, *Ace*-AMP1 is unable to bind diacylphospholipids. These results are in agreement

FIGURE 9: Stereoview of small cavities inside *Ace*-AMP1. The backbone is represented as a gray tube, and aromatic residues are indicated in black. The cavities are shown as dark gray spaces.

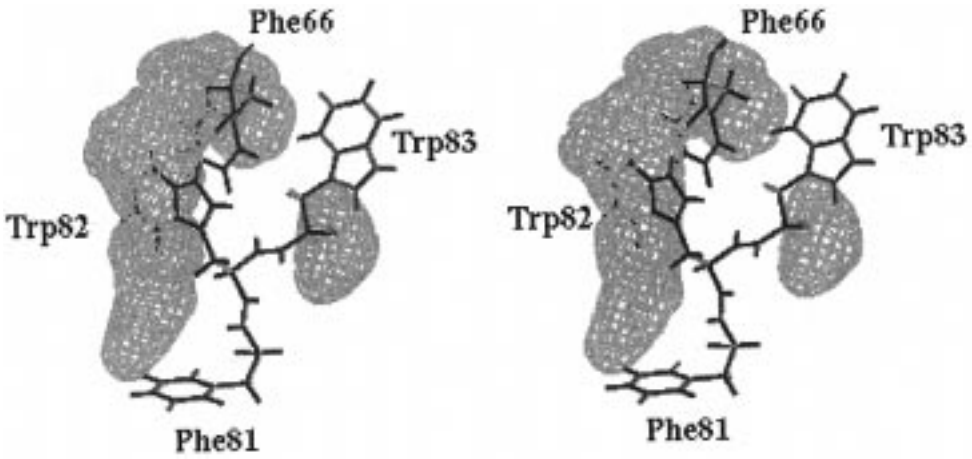

FIGURE 10: Stereoview of the maize ns-LTP cavity with indications of the positions of the aromatic residues of *Ace*-AMP1 (Phe66, Phe81, Trp82, and Trp83).

with previous results which demonstrated that *Ace*-AMP1 could not transfer phospholipids between mitochondria and liposomes (*14*) and with our structural data which show that no cavity is present in this protein. However, *Ace*-AMP1 can interact with bilayer vesicles composed of an anionic phospholipid, phosphatidylglycerol, as shown by fluorescence polarization experiments with fluorescent membrane-embedded probes. This interaction is apparently stronger with *Ace*-AMP1 than with wheat ns-LTP. The decrease in cooperativity of the gel−fluid phase transition of the phospholipid membrane indicates that *Ace*-AMP1 is capable of penetrating slightly into the hydrophobic core of lipid bilayers. This effect is more pronounced with puroindoline-a, a wheat protein structurally related to plant ns-LTPs (*52*) which is capable of deeply penetrating into lipid bilayers (*50*). This is consistent with our observation that puroindoline-a is more efficient than *Ace*-AMP1 in releasing carboxyfluorescein from the lumen of liposomes. Hence, although *Ace*-AMP1 clearly interacts with phospholipid membranes, it is not particularly potent in disturbing or permeabilizing such membranes in comparison to other proteins such as puroindolines. As noted previously (*14*), the antifungal activity of *Ace*-AMP1 cannot be based on lipid transfer activity as the protein is unable to transfer individual lipids. On the other hand, it is also unlikely that *Ace*-AMP1 exerts its antifungal effect by interacting directly with phospholipid membranes. Indeed, if lipid interaction would be the basis of the antifungal activity of *Ace*-AMP1, one would expect puroindolines to exert an even stronger antifungal activity than *Ace*-AMP1. However, antifungal activity assays show that puroindoline-a is significantly less potent than *Ace*-AMP1 in inhibiting fungal growth, especially in the presence of salt (W. F. Broekaert, unpublished results). Another difference between *Ace*-AMP1, both puroindolines, and ns-LTPs is the fact that puroindolines and ns-LTPs can potentiate the antifungal activity of membrane-disturbing proteins called thionins whereas *Ace*-AMP1 cannot (*13*; W. F. Broekaert, unpublished results). For all these reasons, we favor the working hypothesis that *Ace*-AMP1 does not affect fungal growth via direct protein−lipid interactions but rather via protein−lipid interactions mediated by a membrane receptor.

Ace-AMP1 is the only known protein of the ns-LTP family which contains such a high number of positive residues (19 arginines). Maize ns-LTP, for instance, contains only 8 basic residues. In the *Ace*-AMP1 structure, although the arginine residues are well spread all over the sequence, at least 12 of them are oriented toward the C-terminal region. For the maize ns-LTP protein, we have shown that most of these residues are oriented toward the C-terminal region, thus constituting a possible interaction site of ns-LTPs with acidic lipid layers (*20*). Such a conclusion could therefore be extended to *Ace*-AMP1.

In addition to *Ace*-AMP1 and ns-LTPs, other more distantly related proteins also seem to have adopted a folding based on a bundle of four cystine-stabilized α-helixes. These proteins include puroindolines (*52*), 2S albumines (*53*), and probably also related α-amylase/protease inhibitors from

cereal seeds (*54*). It is interesting to note that puroindolines (*52*) and 2S albumines (*55*) have also been shown to interact with phospholipid membranes. Hence, interaction with membranes seems to be a general property of this protein superfamilly, although the way they interact with membranes apparently differs significantly among the different superfamilly members.

In conclusion, the four known three-dimensional structures of proteins extracted from different plant seeds (wheat, maize, barley, and onion) exhibit very similar folds. The organization of their hydrophobic cores appears to be a determinant of their capacity to bind lipids. In proteins from cereal seeds that are actual ns-LTPs, there is an open internal cavity that can readily expand and accommodate various hydrophobic substrates. The presence of such a large cavity in proteins is quite remarkable and raises questions about the folding and the stability of their structures which will be discussed elsewhere (J. Poznanski, unpublished experiments). In *Ace*-AMP1, this cavity is blocked by aromatic residues and the protein neither binds nor transfers lipids. Lipid binding and intermembrane transfer properties are then closely related. It should be now interesting to determine structures of proteins extracted from others seeds and more generally from different parts of plants. It is now established that there are generally several LTP genes per plant genome which encode for isoforms with distinct patterns of expression (*56*, *57*). A systematic analysis of their structures and of the corresponding lipid binding and transfer properties as well as antibacterial and antifungal activities should clarify the biological role of these proteins. On the basis of the extracellular location of the EP2 protein secreted by embryogenic cell cultures of carrot and identified as a LTP, Sterk et al. (*24*) have proposed for this protein a role in the surface defense of plants in which the protein transports cutin monomers to the apoplast. Such a role would be different from lipid transfer between membranes. Preliminary results (D. Marion, personal communication) confirm that ns-LTPs are able to bind such oxygenated fatty acids. Considering that various proteins from microorganisms and from animals with different molecular weights, different specificities, and possibly different structures are also capable of transferring lipids between membranes, this property seems to be rather general and not clearly related to a biological function. Plant ns-LTPs which can bind various lipids and hydrophobic compounds and have various patterns of expression and various locations appear as multifunctional proteins. They could be involved in several different mechanisms of binding and transport of substrates, essential for the development and the surface defense of these plants, toward sites which are not necessarily membranes.

On the basis of the growth inhibition of plant pathogens by several isoforms of barley ns-LTPs (*13*) and on the basis of the antifungal properties of *Ace*-AMP1, a different role has been proposed for other proteins which are structural analogues of ns-LTPs but which would contribute differently to the plant defense by acting on pathogens. This property seems to be more related to their interactions with membrane structures than to their capacity to transfer lipids. The existence of such a family of proteins having similar structures but different functions is puzzling and could indicate that plants use various and potent mechanisms to defend against pathogens and environmental injuries.

ACKNOWLEDGMENT

We thank Geneviève Compoint for her technical assistance in the fluorescence experiments.

SUPPORTING INFORMATION AVAILABLE

Table containing the ^{1}H chemical shifts of *Ace*-AMP1 (2 pages). Ordering information is given on any current masthead page.

REFERENCES

Stuart, L. S., and Harris, T. H. (1942) *Cereal Chem. 19*, 288−300.
Manners, D. J., and Marshall, J. J. (1973) *Phytochemistry 12*, 547−553.
Leah, R., Tommerup, H., Svendsen, I., and Mundy, J. (1991) *J. Biol. Chem. 266*, 1564−1573.
Vigers, A. J., Roberts, W. K., and Selitrennikoff, C. P. (1991) *Mol. Plant−Microbe Interact. 4*, 315−323.
Roberts, W. K., and Selitrennikoff, C. P. (1986) *Biochim. Biophys. Acta 880*, 161−171.
Broekaert, W. F., Mariën, W., Terras, F. R. G., De Bolle, M. F. C., Proost, P., Van Damme, J., Dillen, L., Claeys, M., Rees, S. B., Vanderleyden, L., and Cammue, B. P. A. (1992) *Biochemistry 31*, 4308−4314.
Cammue, B. P. A., De Bolle, M. F. C., Terras, F. R. G., Proost, P., Van Damme, J., Rees, S. B., Vanderleyden, L., and Broekaert, W. F. (1992) *J. Biol. Chem. 267*, 2228−2233.
Duvick, J. P., Rood, T., Rao, A. G., and Marshak, D. R. (1992) *J. Biol. Chem. 267*, 18814−18820.
Terras, F. R. G., Goderis, I. J., Van Leuven, F., Vanderleyden, J., Cammue, B. P. A., and Broekaert, W. F. (1992a) *Plant Physiol. 100*, 1055−1058.
Terras, F. R. G., Torrekens, S., Van Leuven, F., Osborn, R. W., Vanderleyden, J., Cammue, B. P. A., and Broekaert, W. F. (1993) *FEBS Lett. 316*, 233−240.
Terras, F. R. G., Eggermont, K., Kovaleva, V., Raikhel, N. V., Osborn, R. W., Kester, A., Rees, S. B., Vanderleyden, J., Cammue, B. P. A., and Broekaert, W. F. (1995) *Plant Cell 7*, 573−588.
Terras, F. R. G., Schoofs, H. M. E., De Bolle, M. F. C., Van Leuven, F., Rees, S. B., Vanderleyden, J., Cammue, B. P. A., and Broekaert, W. F. (1992b) *J. Biol. Chem. 267*, 15301−15309.
Molina, A., Segura, A., and Garcia-Olmedo, F. (1993) *FEBS Lett. 316*, 119−122.
Cammue, B. P. A., Thevissen, K., Hendriks, M., Eggermont, K., Goderis, I. J., Proost, P., Van Damme, J., Osborn, R. W., Guerbette, F., Kader, J. C., and Broekaert, W. F. (1995) *Plant Physiol. 109*, 445−455.
Nakamura, K., and Matsuoka, K. (1993) *Plant Physiol. 101*, 1−5.
Bednarek, S. Y., and Raikhel, N. V. (1991) *Plant Cell 3*, 1195−1206.
Neuhaus, J. M., Sticher, L., Meins, F., Jr., and Boller, T. (1991) *Proc. Natl. Acad. Sci. U.S.A. 88*, 10362−10366.
Gomar, J., Sodano, P., Ptak, M., and Vovelle, F. (1997) *Folding Des. 2*, 183−192.
Gincel, E., Simorre, J. P., Caille, A., Marion, D., Ptak, M., and Vovelle, F. (1994) *Eur. J. Biochem. 226*, 413−422.
Gomar, J., Petit, M. C., Sodano, P., Sy, D., Marion, D., Kader, J. C., Vovelle, F., and Ptak, M. (1996) *Protein Sci. 5*, 565−577.
Shin, D. H., Lee, J. Y., Hwang, K. Y., Kim, K. K., and Suh, S. W. (1995) *Structure 3*, 189−199.
Heinemann, B., Andersen, K. V., Nielsen, P. R., Bech, L. M., and Poulsen, F. M. (1996) *Protein Sci. 5*, 13−23.
Lerche, M. H., Kragelund B. B., Bech, L. M., and Poulsen, F. M. (1997) *Structure 5*, 291−306.
Sterk, P., Booij, H., Schellekens, G. A., Van Kammen, A., and De Vries, S. C. (1991) *Plant Cell 3*, 907−921.
Garcia-Olmedo, F., Molina, A., Segura, A., and Moreno, M. (1995) *Trends Microbiol. 3*, 72−74.
Petit, M. C., Sodano, P., Marion, D., and Ptak, M. (1994) *Eur. J. Biochem. 222*, 1047−1054.

Record, E., Asther, Mi., Marion, D., and Asther M. (1995) *Biochim. Biophys. Acta 1256*, 18−24.
Wilschut, J. (1982) in *Les Editions INSERM* (Leserman, L. D., and Barbet, J., Eds.) p 137, INSERM, Paris.
States, D. J., Haberkorn, R. A., and Ruben, D. J. (1982) *J. Magn. Reson. 48*, 286−292.
Bax, A., and Davis, D. G. (1985) *J. Magn. Reson. 65*, 355−360.
Marion, D., Ikura, M., and Bax, A. (1989) *J. Magn. Reson. 84*, 425−430.
Shaka, A. J., and Freeman, R. (1983) *J. Magn. Reson. 51*, 169−173.
King, G., and Wright, P. E. (1983) *J. Magn. Reson. 54*, 328−332.
Piotto, M., Saudek, V., and Sklenar, V. (1992) *J. Biomol. NMR 2*, 661−665.
Brown, S. C., Weber, P. L., and Mueller, L. (1988) *J. Magn. Reson. 77*, 166−169.
Nilges, M., Clore, G. M., and Gronenborn, A. M. (1988) *FEBS Lett. 229*, 317−324.
Güntert, P., Braun, W., and Wüthrich, K. (1991) *J. Mol. Biol. 217*, 517−530.
Güntert, P., and Wüthrich, K. (1991) *J. Biomol. NMR 1*, 447−456.
Güntert, P., Berndt, K. D., and Wüthrich, K. (1993) *J. Biomol. NMR 3*, 601−606.
Eccles, C., Güntert, P., Billeter, M., and Wüthrich, K. (1991) *J. Biomol. NMR 1*, 111−130.
Szyperski, T., Güntert, P., Otting, G., and Wüthrich, K. (1991) *J. Magn. Reson. 99*, 552−560.
Brünger, A. T. (1992) *The X-PLOR software manual version 3.1*, Yale University, New Haven, CT.
Brooks, B. R., Bruccoleri, R. E., Olafson, B. D., States, D. J., Swaminathan, S., and Karplus, M. (1983) *J. Comput. Chem. 4*, 187−217.
Hutchinson, E. G., and Thornton, J. M. (1996) *Protein Sci. 5*, 212−220.
Laskowski, R. A., MacArthur, M. W., Moss, D. S., and Thornton, J. M. (1993) *J. Appl. Crystallogr. 26*, 283−291.
Wüthrich, K. (1986) *NMR of proteins and acid nucleics*, Wiley, New York.
Sodano, P., and Ptak, M. (1995) *J. Biomol. Struct. Dyn. 12*, 1009−1022.
Laskowski, R. A., Rullmann, J. A. C., MacArthur, M. W., Kaptein, R., and Thornton, J. M. (1996) *J. Biomol. NMR 8*, 477−486.
Richardson, J. S. (1981) *Adv. Protein Chem. 34*, 168−339.
Dubreil, L., Compoint, J. P., and Marion, D. (1997) *J. Agric. Food Chem. 45*, 108−116.
Sodano, P., Caille, A., Sy, D., de Person, G., Marion, D., and Ptak, M. (1997) *FEBS Lett. 416*, 130−134.
Le Bihan, T., Blochet, J. E., Désormeaux, A., Marion, D., and Pézolet, M. (1996) *Biochemistry 35*, 12712−12722.
Rico, M., Bruix, M., Gonzales, C., Monsalve, R. I., and Rodriguez, R. (1996) *Biochemistry 35*, 15672−15682.
Kreis, M., Forde, B. G., Rahman, S., Miflin, B. J., and Shewry, P. R. (1985) *J. Mol. Biol. 183*, 499−502.
Onaderra, M., Monsalve, R. I., Mancheno, J. M., Villalba, M., Marinez del Pozo, A., Gavilanez, J. G., and Rodriguez, R. (1994) *Eur. J. Biochem. 225*, 609−615.
Fleming, A. J., Mandel, T., Hofman, S., Sterk, P., De Vries, S. C., and Kuhlmeier, C. (1992) *Plant J. 2*, 855−862.
Thoma, S., Hecht, U., Kippers, A., Botella, J., De Vries, S., and Sommerville, C. (1994) *Plant Physiol. 105*, 35−45.
Kraulis, P. J. (1991) *Acta Crystallogr., Sect. B: Struct. Sci. 48*, 115−116.
Tchang, F., This, P., Stiefel, V., Arondel, V., Morch, M. D., Pages, M., Puigdomenech, P., Grellet, F., Delseny, M., Bouillon, P., Huet, J. C., Guerbette, F., Beauvais-Cante, F., Duranton, H., Pernolet, J. C., and Kader, J. C. (1988) *J. Biol. Chem. 263*, 16849−16855.
Désormeaux, A., Blochet, J. E., Pézolet, M., and Marion, D. (1992)-*Biochim. Biophys. Acta 1121*, 137−152.
Mundy, J., and Rogers, J. C. (1986) *Planta 169*, 51−63.
Yu, Y. G., Chung, C. H., Fowler, A., and Suh, S. W. (1988) *Arch. Biochem. Biophys. 265*, 466−475.
Campos, F. A., and Richardson, M. (1984) *FEBS Lett. 167*, 221−225.
Torres-Schuman, S., Gogoy, J. A., and Pintor-Toro, J. (1992) *Plant Mol. Biol. 18*, 749−757.
Masuta, C., Furuno, M., Tanaka, H., Yamada, M., and Koiwai, A. (1992) *FEBS Lett. 311*, 119−123.
Bernhard, W. R., Thoma, S., Botella, J., and Somerville, C. R. (1991) *Plant Physiol. 95*, 164−170.
Soufleri, I. A., Vergnolle, C., Miginiac, E., and Kader, J. C. (1996) *Planta 199*, 229−237.
Pyee, J., and Kolattukudy, P. E. (1995) *Plant J. 7*, 49−59.
Tsuboi, S., Suga, T., Takishima, K., Mamiya, G., Matsui, K., Oseki, Y., and Yamada, M. (1991) *J. Biochem. 110*, 823−831.

BI9723515